Article

Synergistic Effects in a ZnO Powder-Based Coating Sequentially Irradiated with Protons, Electrons, and Solar Spectrum Quanta

Mikhail M. Mikhailov, Semyon A. Yuryev *, Alexey N. Lapin and Vadim V. Karanskiy

Tomsk State University of Control Systems and Radioelectronics, 40 Lenina Ave., 634050 Tomsk, Russia;
membrana2010@mail.ru (M.M.M.); alexey_nl@sibmail.com (A.N.L.); karanskiy2015@mail.ru (V.V.K.)
* Correspondence: semyon.yuryev@tusur.ru

Abstract: The authors investigated the changes in diffuse reflectance spectra (ρ_λ) within 0.32–2.1 μm and integral absorption coefficient (a_s) of solar irradiation for a zinc oxide powder-based coating. The latter was consequently irradiated with protons (E = 3 keV, F $\leq$ 1 $\times$ 10^{16} cm^{-2}), solar spectrum quanta (5 eq. of solar irradiation, 1 h), electrons (E = 30 keV, F = 1 $\times$ 10^{16} cm^{-2}), and—repetitively—solar spectrum quanta (5 eq. of solar irradiation, 1 h). Following the irradiation procedure, the decrease in absorption coefficient varied from 0.044 to 0.036 and from 0.062 to 0.04, respectively. Additionally, it was shown that the solar spectrum quanta did not significantly affect the coating pre-irradiated with protons or electrons and did not change the value of induced absorption in the visible region (the latter being caused by the absorption of intrinsic point defects of the zinc oxide crystal lattice). The absorption coefficient degradation decreased under solar spectrum quanta irradiation, which was determined by the decrease in the concentration of free electrons that absorbed in the near-infrared (near-IR) region. ρ_λ spectra were measured in high vacuum in situ. A post-irradiation transfer of a coating into the atmosphere leads not only to the complete recovery of its reflectance, but also to partial translucence in comparison with the non-irradiated state.

Keywords: synergetics; sequential irradiation; separate irradiation; optical properties; protons; electrons; solar spectrum quanta; zinc oxide

---

1. Introduction

In outer space (OS), various forms of radiation affect external surfaces of spacecraft (SC) either simultaneously or consequently. These materials can be considered as open systems. Changes in their properties are pre-determined by changes of entropy. Methods and principles of synergetics can be used to describe the non-equilibrium system behavior.

Non-equilibrium thermodynamics is based on the entropy balance equation: $dS = dS_1 + dS_2$, where dS_1 and dS_2 stand for entropy flow from external space and its production inside the system, respectively. In an isolated system, $dS_1 = 0$ and $dS_2 \geq 0$. In an open system, dS_1 does not have a definite value, and a system can reach the state where entropy is below the initial value. If a negative entropy flow enters the system, it can maintain an arranged configuration. Such backfeed occurs under non-equilibrium conditions. According to this, non-equilibrium is the source of order.

In the transition to dissipative structures, a symmetry violation leads to ordering near the transition point; thus, the system entropy decreases [1].

Therefore, the system may manifest synergistic effects when several different kinds of OS irradiation affect the SC materials simultaneously or consequently, that is, changes in the properties of materials can differ from the overall change under the separated action of irradiation [2].

The effect of UV light quanta and the visible spectral range on dielectric and semiconductor compounds pre-irradiated with charged particles, gamma quanta, or neutrons has always been of interest to the radiation physics of solids. The purpose of studying this effect is to determine the ionization energy, types, and concentration of impurities contained in such compounds. Spectrophotometry remains one of the most efficient methods for such a purpose. Classic studies employed alkali halid crystals with a cubic lattice [3,4]. As knowledge accumulated, magnesium oxide crystals were chosen as a reference point [5,6].

With the exploration of OS, it became necessary to study the properties and performance characteristics of materials for SC under the simultaneous or sequential action of various types of ionizing radiation. An essential component of ionizing radiation in all orbits is the electromagnetic radiation (EMR) of the Sun, which includes quanta of the UV, visible, and near-IR regions, whose energy is within 0.4 to 6 eV. Such particles can both cause lattice defects in the materials of the SC's outer surfaces and produce their ionization depending on their energy and the band gap (Eg) of the irradiated material.

The solar EMR, electrons, and protons affect simultaneously, sequentially, or separately the materials of the SC's outer surfaces in real SC orbits while circulating around the Earth or other planets. When entering the Earth's shadow, the EMR intensity decreases from maximum to zero. This is a period of charge particles' sole action. The defects are formed by this process when SC leave the Earth's shadow and are subject to EMR quanta. According to the existing concepts of radiation physics, these radiation defects can be "annealed", that is, they can undergo ionization under the influence of quanta with an energy lower than the band gap (Eg) of the compounds.

Thermal control coatings (TCCs) and solar panels (SPs) are the largest in area among the materials of the SC's outer surfaces. Zinc oxide powders are currently used in TCCs [7,8], and studies are underway to clarify the possible use of zinc oxide in SPs [9,10]. To determine the degradation of their structure as well as their optical and electrophysical properties in real orbits, it is necessary to know the laws of formation and accumulation of photo- and radiation defects when exposed to simultaneous, sequential, or separate radiation of various types.

The purpose of this work was to study changes in diffuse reflectance spectra (ρ_λ) upon separate and sequential irradiation of TCCs based on zinc oxide powder by protons → EMR → electrons → EMR.

2. Materials and Methods

The studies were carried out using the TRSO-2M TCC brand based on zinc oxide powder (extra pure, OSC-14-2 in Russian nomenclature by TU-6-09-2175-77, obtained from ZAO Vekton, St. Petersburg, Russia). Sizes of the powder particles were within 0.5–5 µm, with an average of 1.6 µm. Samples were prepared by adding 15 wt.% potassium liquid glass (extra pure, OSC-6-2 in Russian nomenclature by TU-6-09-19-67-72, obtained from OOO NPO "Silikat", St. Petersburg, Russia) with subsequent stirring in a magnetic stirrer, applying the mixture onto metal substrates with a diameter of 24 mm and thickness of 4 mm, and drying in the atmosphere at room temperature for 24–30 h. The air humidity was 40%.

The obtained samples were mounted onto the stage of "Spektr", the OS conditions simulator [11]. A high vacuum was obtained ($p \leq 5 \times 10^{-7}$ torr), and ρ_λ spectra were recorded within 0.32–2.1 µm.

While recording ρ_λ spectra in atmospheric conditions after irradiation, free electrons are consumed by sorbed gases and anionic vacancies were filled with oxygen. Additionally, there were other defects interacting with the gases. Therefore, the concentration of irradiation-induced defects decreased. Significantly lower changes in ρ_λ spectra and integral absorption coefficients were recorded, in comparison with their true values after irradiation of pigments and TCCs in vacuum (in situ) and with the actual values existing in space orbits.

"Spektr", the simulator of space conditions, is designed for studying the diffuse reflectance and luminescence spectra of solids under initial conditions and during (or after) irradiation by light from a

xenon lamp, simulating the spectra of solar electromagnetic irradiation, by electrons (E = 5–150 keV) or by protons (E = 0.5–140 keV). The screen installed in the simulation camera was cooled by liquid nitrogen to simulate "cold dark" space. Up to 24 samples can be loaded into the apparatus simultaneously, and ρ_λ spectra can be registered before and after irradiation without loss of vacuum.

Irradiation of the samples was carried out according to the following scheme: protons → EMR → electrons → EMR.

Irradiation was carried out in three modes.

1. Sample 1, sequential irradiation: protons (E_{p+} = 3 keV, $F_{P+} \leq 1 \times 10^{16}$ cm^{-2}) → EMR (Es = 5 sre, t = 1 h) → electrons (E_{e-} = 30 keV, Φ_{e-} = 1×10^{16} cm^{-2}) → EMR (Es = 5 sre, t = 1 h).

2. Sample 2, separate irradiation: electrons (E_{e-} = 30 keV, $\Phi_{e-} \leq 1 \times 10^{16}$ cm^{-2}).

3. Sample 3, separate irradiation: EMR (Es = 5 sre, t = 40 h).

SRE stands for the solar radiation equivalent that shows the number of times the radiation power is to exceed the solar constant over the entire spectrum (1 sre = 0.137 W/cm^2).

The energy of protons and electrons was chosen for these experimental studies because the solar wind protons fill the entire solar system and their energy is 1–3 keV. Electrons with tens of keV have the highest fluxes in highly elliptical, geostationary, and other orbits passing through the Earth's radiation belts [12,13]. After each irradiation period, the ρ_λ spectra of the irradiated samples were recorded at the irradiation site (in situ).

The spectra ρ_λ allowed the authors to calculate the integral absorption coefficient of solar radiation (a_s), the latter being the TCC performance characteristic. The calculations were carried out in compliance with the standards [14,15]:

$$a_s = 1 - R_s = 1 - \frac{\int_{\lambda_1}^{\lambda_2} \rho_\lambda I_\lambda \mathrm{d}\lambda}{\int_{\lambda_1}^{\lambda_2} I_\lambda \mathrm{d}\lambda}, \tag{1}$$

where R_s is the integral reflectance coefficient of solar radiation, I_λ is the radiation spectrum of the Sun, and (λ_1-λ_2) is the wavelength range of the solar spectrum used for integration, equal to 0.32–2.1 µm.

The values of the absorption coefficient before irradiation (a_{so}) and after a certain fluence of electrons or protons (a_{sf}) were used to calculate the coefficient change ($\Delta a_s = a_{sf} - a_{so}$). Additionally, the authors analyzed the correlations between Δa_s and the electron/proton fluence.

Images of the samples were obtained using a Hitachi *TM-1000* SEM microscope (Tokyo, Japan).

Mathematical modeling of the charged particle paths was conducted via CASINO (monte CArlo SImulation of electroN trajectory in sOlids) (version 3.3.0.4, Universite de Sherbrooke, Sherbrooke, Quebec, Canada) [16] and SRIM (the Stopping and Range of Ions in Matter) (version 2013.00, James F. Ziegler, USA) [17].

CASINO allows one to model a large number of electron paths in solids via the Monte Carlo method, based on different models. The basic idea is modeling electron trajectories sufficiently to represent conditions of displaying structures in SEM.

SRIM is software designed to calculate interactions of ions with matter. SRIM is popular in the research community working on ionic implantation technologies, and is also widely used in other areas of radiation materials science.

Because the amount of binder was relatively small compared with that of the pigment, a ZnO compound with a density of 5.6 g/cm^3 was applied as a target during modeling for simplicity and visibility. While working in CASINO, the specified energy of electrons was 30 keV, while the beam diameter was 1 nm. For modeling in SRIM, the specified energy for protons (i.e., hydrogen ions) was 3 keV.

3. Results and Discussion

Figure 1 shows images of the initial ZnO powder and the coating prepared on its base. After drying the coating on a substrate, a smooth sample was obtained. The surface of the latter reproduced the surface of ZnO powder particles. The thickness of the obtained coating was 150 µm, which is a

standard thickness for classic TCCs. As can be seen from Figure 1, the addition of potassium liquid glass improves the even distribution of the ZnO powder particles.
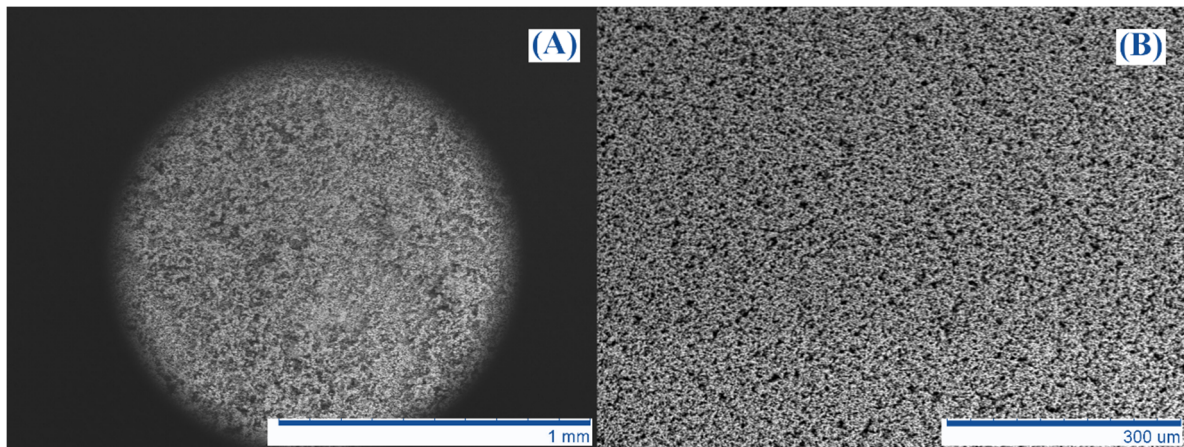
Figure 1. (**A**) SEM images of ZnO powder and (**B**) coating obtained by addition of 15 wt.% of potassium liquid glass.

The authors conducted mathematical modeling of the charged particle paths (Figure 2) via CASINO for electrons and SRIM for protons. The results show that the path value for 30 keV electrons is much higher than that for 3 keV protons in the zinc oxide powder. As can be seen from Figure 2, the maximum path value is 3 μm for electrons and 110 nm for protons. As for the combined action of the oppositely charged particles, it is carried out in a 110 nm thick layer, which is 27.3 times as small as the depth of the layer damaged by electron irradiation.
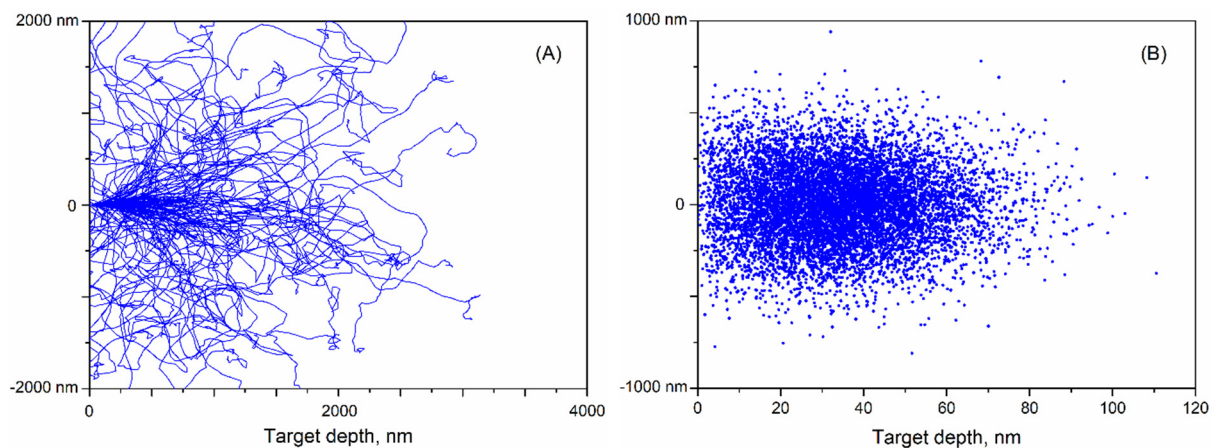
**Figure 2.** (**A**) Modeling the path for electrons of 30 keV and (**B**) protons of 3 keV in zinc oxide.

3.1. Sample 1: $(p^+ \rightarrow EMR)$ Irradiation Mode

As seen from the ρ_λ spectrum of the initial TCC (Figure 3), the main absorption edge corresponds to 375 nm. In the longer wavelength region, the reflectance coefficient (ρ) increases and exceeds 90% at 450 nm. Then, it undergoes a smooth insignificant decrease to 1400 nm, whereas in the longer wavelength region it sharply decreases, being 65% at 2100 nm.
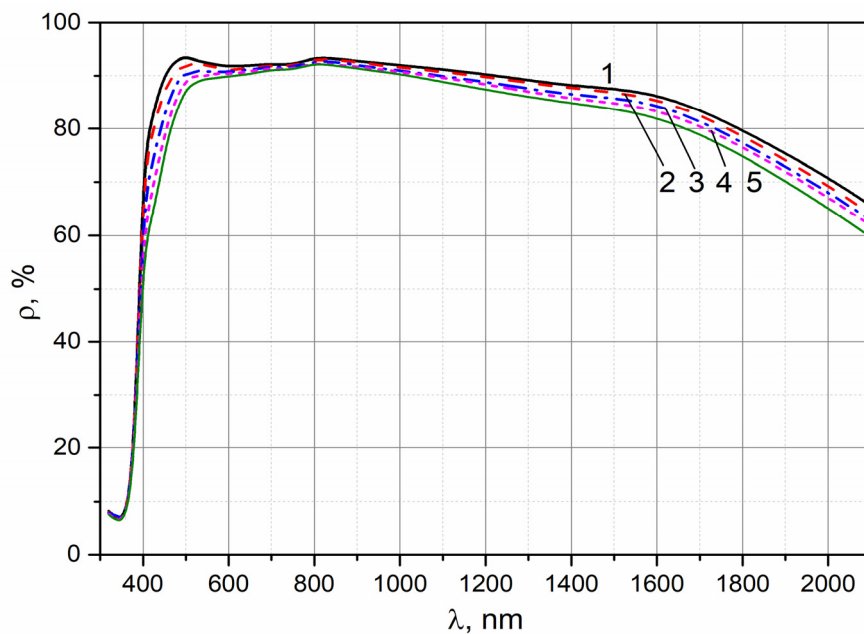
Figure 3. ρ_λ spectra before (1) and after irradiation of the TRSO-2M coating with a 3 keV proton fluence: 1×10^{15} (2), 3×10^{15} (3), 6×10^{15} (4), and 1×10^{16} (5).

After irradiation with a proton fluence of 1×10^{15} cm^{-2}, the reflectance coefficient decreases by 3% in the visible region, while in the near-IR region the changes are even smaller. With an increase in the proton fluence, the changes in ρ increase mainly in the visible region. In the difference spectra (obtained by subtracting the post-irradiation spectra from the pre-irradiation spectra, $\Delta\rho$), an absorption band is formed with a maximum at 410 nm (Figure 4).
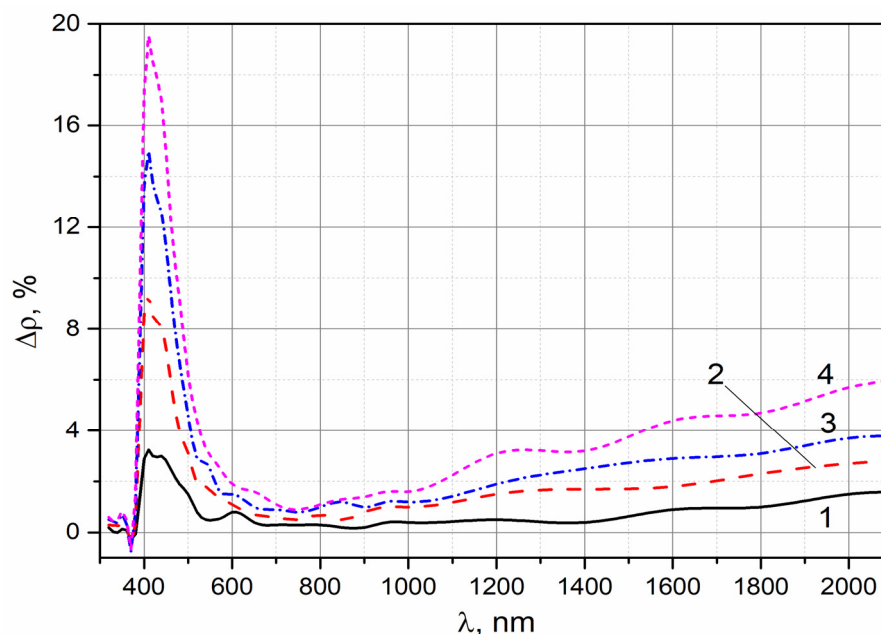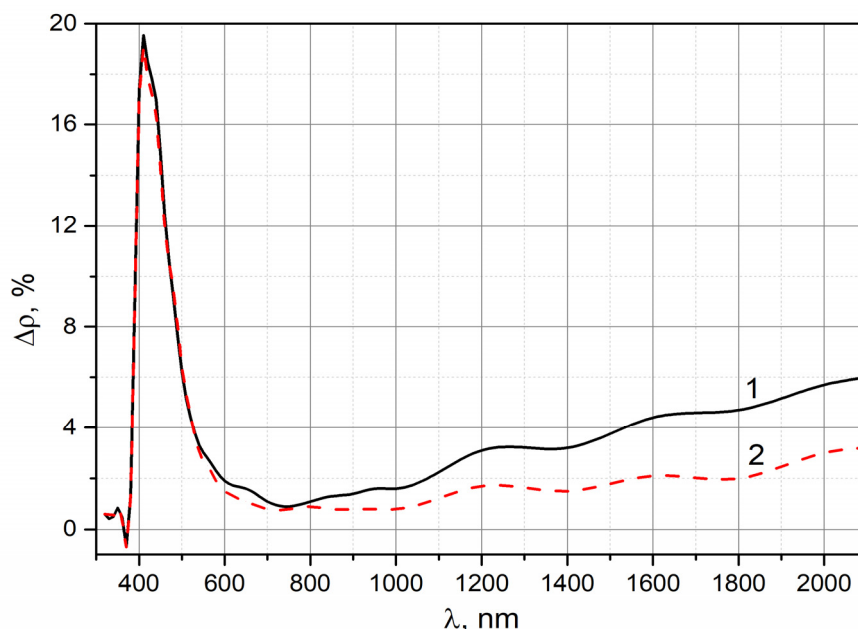

Figure 4. $\Delta\rho_\lambda$ spectra after irradiation of the TRSO-2M coating with a 3 keV proton fluence: 1×10^{15} (1), 3×10^{15} (2), 6×10^{15} (3), and 1×10^{16} (4).

The intensity of this band increases with increasing proton fluence and reaches 19.5% at its maximum value (F = 1×10^{16} cm^{-2}).

In the near-IR region, the changes in ρ increase with higher wavelengths. As proton fluence increases, they become more significant. However, the absolute Δρ values in this region are not large; the maximum value at λ = 2100 nm is 6%.

Subsequent EMR for 1 h with an intensity of 5 sre leads to a very small (0.5%) increase in the reflectance coefficient within the band at 410 nm (Figure 5). In the near-IR region, an increase in the reflectance coefficient occurs (up to 2–3%), that is, reflectance is recovered.

Figure 5. $\Delta\rho_\lambda$ spectra after irradiation of the TRSO-2M coating with a 3 keV proton fluence of 1×10^{16} (1) and after sequential EMR (2).

3.2. Sample 1: ($e_- \to$ EMR) Irradiation Mode after the Action of Protons and EMR

Irradiation by electrons after the action of EMR does not change Δρ at the maximum of the band at 410 nm (Figure 6). In this case, an increase in Δρ values is recorded on its long wavelength wing with the formation of an additional band at approximately 580–600 nm. In the near-IR region, Δρ values increase significantly as wavelength increases, reaching 11.5% at λ = 2100 nm.

Then, 1 h long EMR irradiation followed by exposure to electrons (with the same intensity as protons) leads to the same Δρ values in the near-IR region of the spectrum as its post-proton irradiation effect. Reflectance—previously reduced by electron irradiation—is recovered. The parameters of the band in the visible region are not changed.

Thus, sequential irradiation according to the scheme ($p^+ \to$ EMR $\to e^- \to$ EMR) results in the following changes in the diffuse reflectance spectra of a coating based on zinc oxide powder:

- the exposure to protons forms an absorption band in the visible region with a maximum at 410 nm with a Δρ value of up to 19.5%. The latter increases to 6% with an increase in absorption wavelength;
- the exposure to EMR leads to an almost complete "annealing" of defects that absorb in the near-IR region. However, it does not change the concentration of defects that absorb in the visible region of the spectrum;
- the exposure to electrons not only recovers the $\Delta\rho_\lambda$ spectrum of the near-IR region induced by exposure to protons and "destroyed" by exposure to EMR, but also significantly increases the Δρ values, while maintaining its correlation with the wavelength;
- the subsequent action of EMR leads to qualitatively similar changes in the $\Delta\rho_\lambda$ spectrum to the changes after irradiation with protons. The changes in the visible region are absent. In the near-IR region, defect "annealing" occurs being induced by exposure to electrons.
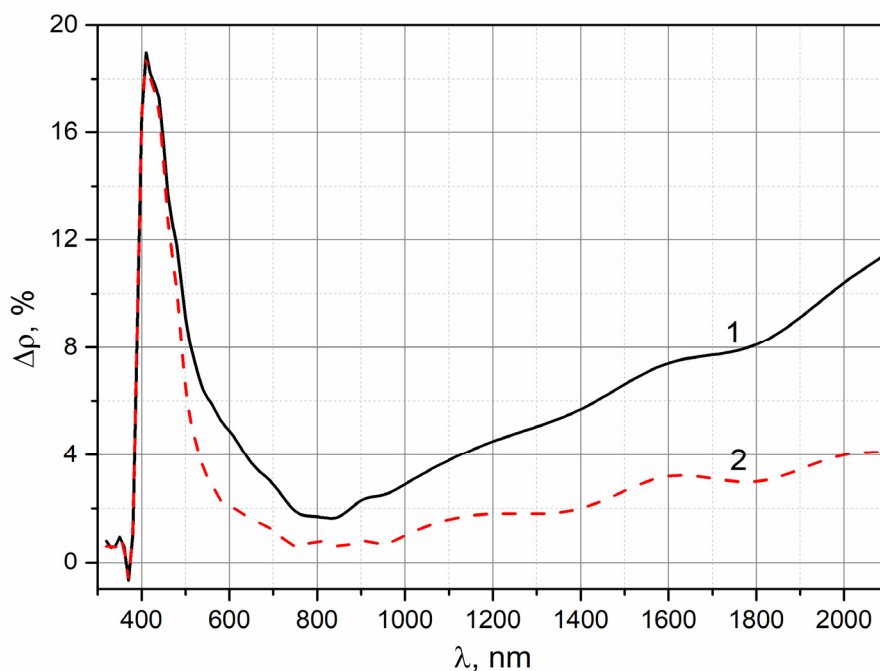
Figure 6. $\Delta\rho_\lambda$ spectra after irradiation of the TRSO-2M coating with 3 keV protons with an energy of $1\cdot10^{16}$ and after sequential irradiation with EMR, electrons (1), and follow-up EMR (2).

3.3. Sample 2: Electron Irradiation of the Initial Powder

The authors separately irradiated the powder with electrons to elucidate the processes that occur during the defect "annealing" via radiation from a xenon arc lamp, which simulated the solar absorption spectrum in the near-IR region. Figure 7 shows the difference spectra obtained after irradiation with electron fluence (F = (0.6–10) × 10^{15} cm^{-2}).
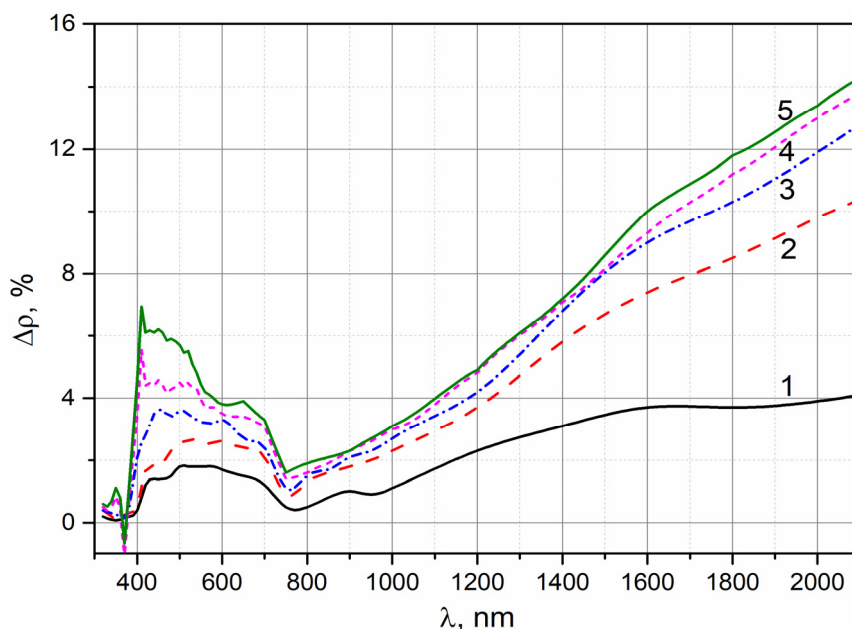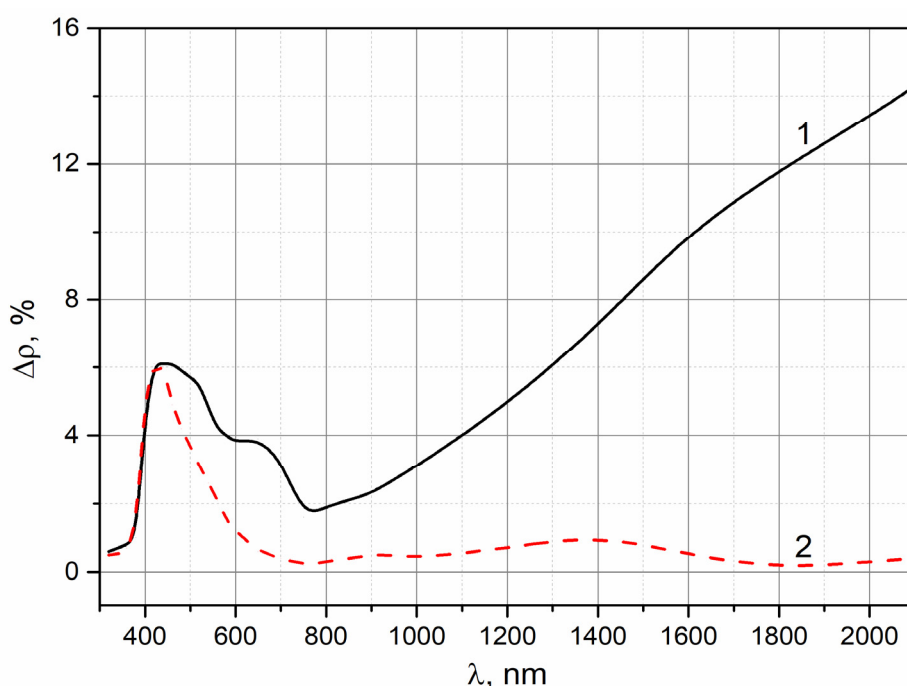

Figure 7. $\Delta\rho_\lambda$ Spectra after irradiation of a TRSO-2M coating with 30 keV electrons, fluence values = $0.6\cdot10^{15}$ (1), 2 × 10^{15} (2), 4 × 10^{15} (3), 6 × 10^{15} (4), and 1 × 10^{16} (5) cm^{-2}.

As seen from the figure, electrons of such energy lead to insignificant changes in the ρ_λ spectrum in the visible region—the maximum $\Delta\rho$ value reaches 7% at the highest fluence F = 1 × 10^{16} cm^{-2}.

In this case, several absorption bands are notable in this region. In the near-IR region, it reaches 13.8% with a fluence of $6 \cdot 10^{15}$ cm^{-2} at a wavelength of 2100 nm, that is, approximately the same value as when pre-irradiated with protons and EMR and exposed to electrons (Figure 6). The peak $\Delta \rho$ value reaches 14.3% at F = 1×10^{16} cm^{-2}.

Regardless of the powder state (i.e., the initial one or sequentially pre-irradiated with protons and EMR), the degradation of the reflectance spectrum in the near-IR region remains the same. In the visible region, this similarity is not maintained—after proton exposure, electrons do not increase the intensity of the main absorption band at 410 nm, while the effect of electrons on the initial powder leads to a decrease in the reflectance coefficient to 7%.

Further irradiation of this sample with EMR quanta in the same mode as for sample 1 leads to almost complete "annealing" of defects that absorb in the near-IR region. In contrast to sample 1 (Figure 6), the annealing of sample 2 is stronger (Figure 8).
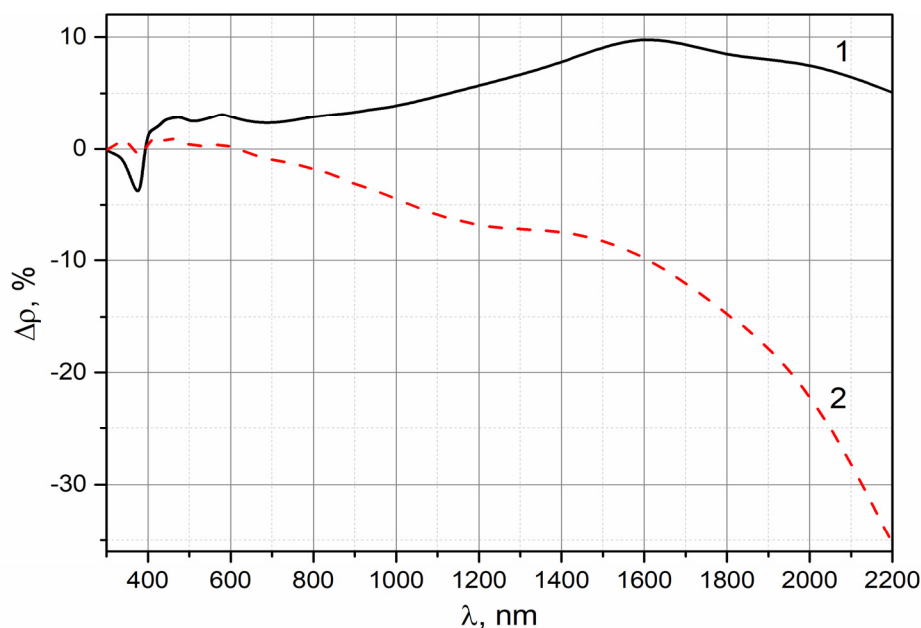

Figure 8. $\Delta \rho_\lambda$ spectra after irradiation of a TRSO-2M coating with 30 keV electrons, F = 1×10^{16} (1) and after sequential irradiation with EMR (2).

3.4. Sample 3: EMR Irradiation of the Initial Powder

The changes in the ρ_λ spectra under the influence of EMR (after irradiating samples 1 and 2 with protons and electrons) demonstrated that the effect of solar spectrum quanta causes a decrease in irregularities induced by pre-irradiation with charged particles. Such "treatment" refers mainly to defects absorbing in the near-IR region. As for the defects absorbing in the visible spectral region within a long wavelength band wing, the above-mentioned treatment is comparatively insignificant. It is of interest to examine the effect of the solar EMR on the diffuse reflectance spectra of the coating.

For this purpose, the initial powder was irradiated with EMR (sample 3) for 40 h with 5 sre intensity. The subsequent degradation in the visible region did not exceed 3% and reached 10% in the near-IR region (Figure 9).

Figure 9. $\Delta\rho_\lambda$ spectra after irradiation of ultra-high purity ZnO 14-2 pigment with 5 sre for 40 h (1) and follow-up 33-day-long storage in a residual vacuum (2).

Comparing the spectra of Figures 7–9 demonstrates that the separate exposure of zinc oxide powder-based TCCs to EMR results in a degradation of the diffuse reflectance spectrum that is qualitatively similar to the one induced by exposure to electrons. Small changes in the reflectance coefficient ρ occur in the visible region, and significant changes occur in the near-IR region. The structure of absorption bands also coincides after exposure to these radiation types.

The effect of atmospheric gases on zinc oxide powder is of interest when irradiated by solar spectrum quanta. A 33-day-long exposure of the irradiated coating leads not only to the recovery of reflectance in the visible and near-IR regions, but also to its translucence, that is, the post-exposure ρ values become larger than the initial ones (Figure 9). The maximum increase in reflectance coefficient reaches 35% at 2100 nm.

3.5. Formation of Intrinsic Point Defects under EMR

As seen from the previous studies [18,19] on the $\Delta\rho_\lambda$ spectra of irradiated zinc oxide powders and TCCs made on their basis, the induced absorption in the visible region is determined by intrinsic point defects of the crystal lattice (i.e., vacancies and interstitial cations/anions of oxygen and zinc in various charge states). For this study, the analysis was carried out for zinc oxide pigment under the assumption that the processes would be qualitatively identical for the TRSO-2M coating itself, the latter containing 85% of this pigment.

The ionization energy of these defects is as follows: eV: Zn_i^{2+}-3.13, V_o^+-3.03, V_{Zn}^--2.83, $(V_{Zn-}$-$Zn_i^o)$-2.64, V_o^o-2.44, $K(V_o)$-2.05, $K_1(V_{Zn})$-1.86, $K_2(V_{Zn})$-1.64, V_{Zn}^o-1.25, V_O^{2+}-1.05, where $K(V_o)$, $K_1(V_{Zn})$, and $K_2(V_{Zn})$ stand for the complexes of point defects based on oxygen and zinc vacancies [18,20,21]. At high fluences of charged particles or EMR doses, small colloid centers and zinc colloids may form inside the zinc oxide powder [19].

In the near-IR region, absorption is determined by free electrons. Their energy distribution in the conductivity band occurs in accordance with a power law. Therefore, the action of solar EMR after the formation of such defects—induced by irradiation with protons or electrons—leads to a decrease in the concentration of free electrons and does not change the concentration of intrinsic point radiation defects.

The solar radiation spectrum includes UV, visible, and near-IR regions. The integral radiation intensity is 0.137 W/cm^2 [14]. The main absorption edge of zinc oxide at room temperature is assigned to 375 nm (Figure 3). The region $\lambda \leq 375$ nm contains 6.5% of quanta of the entire spectrum energy, which is 0.009 W/cm^2. The longer wavelength region contains 93.5% of these quanta (Figure 10), which is equal to 0.128 W/cm^2.
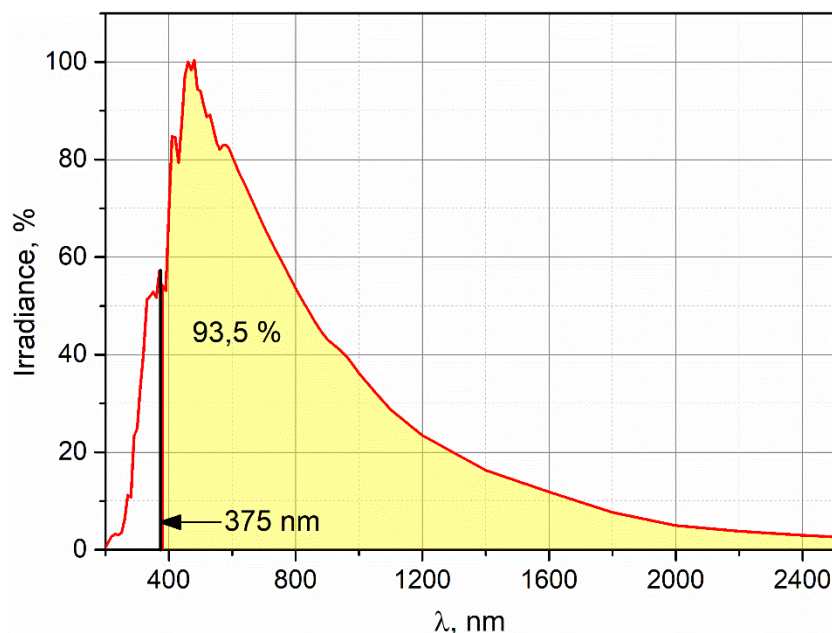
Figure 10. Solar radiation spectrum: 93.5% of quanta has an energy lower than the zinc oxide band gap (375 nm).

With a lamp emission intensity of 5 sre, the radiation power is W = 2340 J/cm^2 or 1.46×10^{22} eV/cm^2 for a 1 h irradiation period. The power is transferred by quanta with energies lower than the zinc oxide band gap; in this case its value equals 3.3 eV, which correlates with the data of the other authors [22].

Such quanta cannot form electron–hole pairs by transferring electrons from the valence band to the conductivity band. They can solely interact with crystal lattice defects that are located in the band gap. Since the powder under investigation has high purity, then—at the beginning of the irradiation period—these quanta can heat solely microcrystalline powder grains. Only 6.5% of the lamp's entire emission spectrum can form ionization defects.

3.6. Recovering of Diffuse Reflectance Spectra by EMR

If quanta with E < Eg affect ZnO powder that was pre-irradiated with protons or electrons (i.e., the one that already contains intrinsic point defects), they can interact with these defects. This can reduce their concentration and the intensity of the related absorption bands in the visible region. In addition, they interact with free electrons formed by pre-irradiation with protons or electrons, as well as with phonons.

If we average the value of the levels of intrinsic point defects in ZnO to half-width of the band gap, that is, 1.65 eV, the number of quanta capable of ionizing crystal lattice defects will be 8.8×10^{21} cm^{-2}.

Thus, the estimation shows that we can form intrinsic crystal lattice defects by irradiating the initial TCC based on zinc oxide powder with the light of a xenon lamp simulating the solar radiation spectrum. The initial stage of this process is the formation of electrons and holes; 6.5% of all radiation is spent on this process. The bulk of radiation quanta (93.5%) does not have sufficient energy to initiate this process and can interact solely with previously formed lattice point defects and phonons.

Free electrons (as any other charged particle) can neither absorb energy from a light wave, nor radiate energy into this wave. An electron can receive only a small recoil energy in light scattering. Absorption of photons directly by conductivity electrons is possible only in simultaneous collisions of electrons with crystal lattice nodes, phonons, defects of various kinds, and grain boundaries, and with each other [23]. Therefore, the subsequent absorption of quanta with an energy smaller than the ZnO band gap involves intrinsic point defects and phonons for zinc oxide powders pre-irradiated with protons or electrons and containing free electrons.

The absorption of photons by defects of the crystal lattice leads to their excitation. The transition to the equilibrium state is accompanied by luminescence, emission of phonons, or impact ionization (Auger effect).

Therefore, the decrease in absorption ($\Delta\rho$ values) recorded in the near-IR region of the spectrum (absorption by free electrons under the solar spectrum quanta in TCCs based on zinc oxide powder previously irradiated by protons or electrons) can be determined by several of the above processes. Studying these processes will deepen the concept of synergistic effects caused by the combined exposure of space technology materials to various types of radiation.

3.7. Change in the Integral Absorption Coefficient

The integral absorption coefficient is the main performance characteristic of TCCs. Table 1 provides its variation during sequential irradiation of the TRSO-2M coating according to the following scheme: $p^+ \rightarrow EMR \rightarrow e- \rightarrow EMR$.

Table 1. Change in the absorption coefficient a_s during sequential irradiation of the TRSO-2M coating ($p^+ \rightarrow EMR \rightarrow e- \rightarrow EMR$).

	Protons				EMR	e^-	EMR
F, cm^{-2}	1×10^{15}	3×10^{15}	6×10^{15}	1×10^{16}	1 h	1×10^{16}	1 h
Δa_s	0.009	0.021	0.032	0.044	0.036	0.062	0.04

The data from Table 1 demonstrates that the exposure to EMR for 1 h leads to a decrease in Δa_s from 0.044 to 0.036 and from 0.62 to 0.04 for the coating pre-irradiated with protons (E = 3 keV, F = 1×10^{16} cm^{-2}) and electrons (E = 30 keV, F = 1×10^{16} cm^{-2}), respectively. With a short EMR exposure time, the decrease is significant, reaching 1.22 and 1.55 times for the TRSO-2M coating pre-irradiated with protons and electrons, respectively.

Degradation within the spectrum significantly differs in both cases, that is, Δa_s = 0.044 after irradiation by protons and Δa_s = 0.062 after irradiation by electrons. Recovery value also differs by a factor of three, namely, by 0.008 in the first case and by 0.022 in the second case.

The degradation decrease and reflectance recovery lead to the final degradation values being close for both modes, that is, 0.036 and 0.04, respectively.

The obtained feature of degradation and reflectance recovery indicates that defects of system symmetry occurring in preliminary irradiation by electrons or protons lead to ordering in the subsequent irradiation by solar spectrum quanta. Thus, system entropy is bound to decrease [1].

4. Conclusions

Studying changes in optical properties upon separate and sequential irradiation with 3 keV protons, 30 keV electrons, and solar spectrum quanta showed the presence of synergistic effects for the TRSO-2M coating based on zinc oxide powder. The exposure of the coating (pre-irradiated with protons and electrons) to the solar spectrum quanta leads to a decrease in the degradation of the diffuse reflectance spectra in the near-IR region because of the absorption by free electrons. Subsequent atmospheric exposure of the coating irradiated in vacuum leads not only to a complete

recovery of reflectance in the near-IR region of the spectrum, but also to its increase compared with the initial state.

The effect of solar spectrum quanta on the coating irradiated by protons or electrons almost does not change the value of the induced absorption in the visible region. The intensity of the integral absorption band at 410 nm caused by intrinsic point defects of the ZnO crystal lattice does not change.

A decrease in the integral absorption coefficient, which is the main performance characteristic of the TCC, can be significant upon irradiation with solar spectrum quanta followed by irradiation with protons or electrons. Thus, the exposure to solar spectrum quanta for 1 h leads to a decrease in Δa_s from 0.044 to 0.036 and from 0.62 to 0.04 for the coating previously irradiated with protons (E = 3 keV, F = 1×10^{16} cm^{-2}) and electrons (E = 30 keV, F = 1×10^{16} cm^{-2}), respectively.

Author Contributions: Conceptualization, M.M.M.; Formal analysis, S.A.Y. and A.N.L.; Funding acquisition, M.M.M.; Investigation, A.N.L. and V.V.K.; Project administration, M.M.M.; Software, S.A.Y.; Validation, A.N.L.; Visualization, S.A.Y. and A.N.L.; Writing—original draft, M.M.M.; Writing—review and editing, S.A.Y. All authors have read and agreed to the published version of the manuscript.

Conflicts of Interest: The authors declare no conflict of interest. The funders had no role in the design of the study; in the collection, analyses, or interpretation of data; in the writing of the manuscript; or in the decision to publish the results.

References

1. Glansdorff, P.; Prigogine, I. *Thermodynamic Theory of Structure, Stability, and Fluctuations*, 1st ed.; Wiley-Interscience: New York, NY, USA, 1971; 306p.
2. Vanina, E.A. Self-organization and Ordering in Oxide and Silicate Systems. Ph.D. Thesis, Amur State University, Blagoveschensk, Russia, 2006. (In Russian)
3. Seitz, F. Color Centers in Alkali Halide Crystals. *Rev. Mod. Phys.* **1946**, *18*, 384–408. [CrossRef]
4. Pick, H. Color centers in alkali halides. *Nuovo Cimento* **1958**, *7*, 498–522. [CrossRef]
5. Wertz, J.E.; Auzins, P.; Weeks, R.A.; Silsbee, R.H. Electron Spin Resonance of F Centers in Magnesium Oxide; Confirmation of the Spin of Magnesium-25. *Phys. Rev.* **1957**, *107*, 1535–1537. [CrossRef]
6. Soshea, R.W.; Dekker, A.J.; Sturtz, J.P. X-ray-induced color centers in MgO. *J. Phys. Chem. Solids* **1958**, *5*, 23–33. [CrossRef]
7. Heydari, V.; Bahreini, Z. Synthesis of silica-supported ZnO pigments for thermal control coatings and analysis of their reflection model. *J. Coat. Technol. Res.* **2018**, *15*, 223–230. [CrossRef]
8. Bo, Z.; Gang, L.; Kangli, C.; Weimin, C. Preparation and Space Environmental Stability of a Nano-Materials Modified Thermal Control Coating. Protection of Materials and Structures from the Space Environment. *Astrophys. Space Sci. Proc.* **2017**, *47*, 433–441. [CrossRef]
9. Tyona, M.D. Doped Zinc Oxide Nanostructures for Photovoltaic Solar Cells Application. In *Zinc Oxide Based Nano Materials and Devices*; IntechOpen: London, United Kingdom, 2019. [CrossRef]
10. Kumari, M.; Kundu, V.S.; Kumar, S.; Chauhan, N.; Siwatch, S. Synthesis, characterization and dye-sensitized solar cell application of Zinc oxide based coaxial core-shell heterostructure. *Mater. Res. Express* **2019**, *6*, 085050. [CrossRef]
11. Kositsyn, L.G.; Mikhailov, M.M.; Kuznetsov, N.Y.; Dvoretskii, M.I. Apparatus for Study of Diffuse—Reflection and Luminescence Spectra of Solids in Vacuum. *Instrum. Exp. Tech.* **1985**, *28 Pt 2*, 929–932.
12. Yu, Y.; Rastatter, L.; Jordanova, V.; Zheng, Y.; Engel, M.; Fok, M.-C.; Kuznetsova, M. Initial results from the GEM challenge on the spacecraft surface charging environment. *Space Weather* **2019**, *17*, 299–312. [CrossRef]
13. Sajid, M.; Chechenin, N.G.; Torres, F.S.; Khan, E.U.; Agha, S. Space radiation environment prediction for VLSI microelectronics devices onboard a LEO Satellite using OMERE-TRAD software. *Adv. Space Res.* **2015**, *56*, 314–324. [CrossRef]
14. *ASTM E490—00a Standard Solar Constant and Zero Air Mass Solar Spectral Irradiance Tables*; ASTM International: West Conshohocken, PA, USA, 2014.

15. *ASTM E903—12 Standard Test Method for Solar Absorptance, Reflectance, and Transmittance of Materials Using Integrating Spheres*; ASTM International: West Conshohocken, PA, USA, 2012.

16. Demers, H.; Poirier-Demers, N.; Réal Couture, A.; Joly, D.; Guilmain, M.; de Jonge, N.; Drouin, D. Three-dimensional electron microscopy simulation with the CASINO Monte Carlo software. *Scanning* **2011**, *33*, 135–146. [CrossRef] [PubMed]

17. Ziegler, J.F.; Ziegler, M.D.; Biersack, J.P. SRIM—The stopping and range of ions in matter. *Nucl. Instrum. Methods Phys. Res. Sect. B* **2010**, *268*, 1818–1823. [CrossRef]

18. Neshchimenko, V.; Li, C.; Mikhailov, M.; Lv, J. Optical radiation stability of ZnO hollow particles. *Nanoscale* **2018**, *10*, 22335–22347. [CrossRef] [PubMed]

19. Mikhailov, M.M.; Neshchimenko, V.V. Characteristic features of colloid centers in the absorption spectra of preliminarily heated zinc oxide powders irradiated by protons. *J Surf. Investig. X-ray Synchrotron Neutron Tech.* **2015**, *9*, 144–152. [CrossRef]

20. Xu, P.S.; Sun, Y.M.; Shi, C.S.; Xu, F.Q.; Pan, H.B. The electronic structure and spectral properties of ZnO and its defects. *Nucl. Instrum. Methods Phys. Res. Sect. B* **2003**, *199*, 286–290. [CrossRef]

21. Erhart, P.; Albe, K.; Klein, A. First-principles study of intrinsic point defects in ZnO: Role of band structure, volume relaxation, and finite-size effects. *Phys. Rev. B* **2006**, *73*, 205203. [CrossRef]

22. Znaidi, L. Sol–gel-deposited ZnO thin films: A review. *Mater. Sci. Eng. B* **2010**, *174*, 18–30. [CrossRef]

23. Vavilov, V.S. *Effects of Radiation on Semiconductors*; Springer: New York, NY, USA, 1965; 225p. [CrossRef]